Seismic behavior of strengthened reinforced concrete coupling beams by bolted steel plates, Part 1: Experimental study

Y. Zhu[†]

Earthquake Engineering Research Test Centre, The University of Guang Zhou, China

R. K. L. Su[‡]

Department of Civil Engineering, The University of Hong Kong, Hong Kong, China

F. L. Zhou[‡†]

Earthquake Engineering Research Test Centre, The University of Guang Zhou, China

Abstract. An experimental study of five full-scale coupling beam specimens has been conducted to investigate the seismic behavior of strengthened RC coupling beams by bolted side steel plates using a reversed cyclic loading procedure. The strengthened coupling beams are fabricated with different plate thicknesses and shear connector arrangements to study their respective effects on load-carrying capacity, strength retention, stiffness degradation, deformation capacity, and energy dissipation ability. The study revealed that putting shear connectors along the span of coupling beams produces no significant improvement to the structural performance of the strengthened beams. Translational and rotational partial interactions of the shear connectors that would weaken the load-carrying capacity of the steel plates were observed and measured. The hierarchy of failure of concrete, steel plates, and shear connectors was identified. Furthermore, detailed effects of plate buckling and various arrangements of shear connectors on the post-peak behavior of the strengthened beams are discussed.

Keywords: coupling beam; strengthening; seismic behavior; steel plate; bolt connection.

1. Introduction

Modern cities like GuangZhou and Hong Kong have numerous old reinforced concrete (RC) buildings which often require substantial strengthening, retrofitting, or refurbishment as the materials used in their construction age. Many local RC buildings were built three or four decades ago, and their concrete and reinforcement have already suffered serious deterioration due to

---

† Lecturer
‡ Assistant Professor, Corresponding author, E-mail: klsu@hkucc.hku.hk
‡† Professor

carbonation and chloride attack. Major retrofitting is normally required for these buildings. Furthermore, several existing buildings designed according to outdated design standards are deficient in shear reinforcement, and require substantial strengthening to increase their safety margin. Recent seismic hazard studies have revealed that Hong Kong is located in a region of low-to-moderate seismicity, and the latest design standards include increased load specifications. Many existing buildings were designed without any provision for earthquake resistance, and are now considered structurally inadequate. As a result, the limited deformability and energy dissipation of existing structures, particularly their coupling beams, which connect the individual shear wall piers together to form a coupled shear wall or core wall, have become a major concern for many local structural and seismic engineers.

The stiffness, strength and ductility of those coupling beams have great influences on the overall structural behavior of coupled wall buildings under seismic attack (Chaallal *et al.* 1996, Subedi *et al.* 1999, Harries 2001). A local failure of coupling beams may lead to a more serious global failure of the whole lateral load resisting system of the building (Stafford Smith and Coull 1991 and Wang *et al.* 1992). Coupling beams usually span a short distance and are relatively deep and, therefore, their structural behavior is not similar to that of common flexural RC beams (Paulay and Bull 1971, Subedi 1991, Pala and Ozmen 1995). A number of researchers (Tassios *et al.* 1996, Tegos and Penlis 1988, Galano and Vignoli 2000, and Kwan and Zhao 2002a) experimentally studied the behavior of coupling beams reinforced with different reinforcement layouts under seismic conditions. Their research revealed that diagonal bar or inclined bar arrangement radically changed the load resisting mechanism and significantly improved the energy dissipation capacity of coupling beams. The aforementioned experiments on the behavior of various coupling beams are useful in the design of new coupling beams. However, for existing substandard coupling beams, retrofitting or strengthening has rarely been reported.

Employing external steel plates to strengthen RC components such as columns, beams or slabs has been widely used in recent years since their first application in the 1960s (L'Hermite and Bresson 1967) for repairing or upgrading RC structures. Many researchers (Jones *et al.* 1982, Taljsten 1995, Oehlers and Moran 1989, Oehlers 1992, Oehlers *et al.* 2000a and b, Lin and Kao 2003) conducted research on strengthening flexural floor beams with bolted or bonded steel plates. It should be noted that bonded-on steel plates for strengthening RC beams always result in high stress concentrations and peeling forces at the ends of the bonded plates. Furthermore, the addition of the plate as for tension reinforcement reduces the ductility of the beam. Consequently, premature and brittle failure modes, namely plate debonding, peeling and separation, often occur (Oehlers and Moran 1989, Oehlers 1992). Several researchers (Subedi and Baglin 1998, Foley and Buckhouse 1999, Ahmed *et al.* 2000, Barnes *et al.* 2001, Uy 2002) have studied the ways to enhance the flexural/shear resistance of concrete beams by means of adhesively bolted steel plates on the soffit/sides of the beams. An improvement of the shear and flexural strengths of the concrete beams was observed. The shear failure of externally plated beams is characterized by a gradual and ductile behavior, in contrast to a typical brittle failure of conventionally reinforced concrete coupling beams. Sufficient plate anchorage is needed to assure the achievement of enhanced shear capacity of the strengthened beams.

With regard to the retrofitting of reinforced concrete coupling beams, Harries *et al.* (1996) had reported their research on seismic retrofitting of RC coupling beams using steel plates. In their research, the retrofitting measures involved the use of adhesive bonding and bolting to fix the thin steel plates to one side of the coupling beams for improving the shear performance. Altogether, four

specimens were tested. The load-ductility curves, failure mechanisms, as well as strength predictions based on modified compression theory (Collins and Mitchell 1991) were presented. Only a relatively low shear strength enhancement of up to 3 MPa was achieved. The effects of bolt slippage and stiffness degradation were not considered. The authors (Su and Zhu 2005) had conducted a preliminary experimental and numerical study of plate strengthened RC coupling beams. The study showed that external steel plates attached by bolted connections could considerably enhance the strength and deformation capacity of coupling beams under reversed cyclic loadings and steadily sustain most of the shear force after reaching the peak loading of the coupling beam. A relatively high shear stress capacity of up to 6.5 MPa was reported for the plate-strengthened beams. The good inelastic responses of the strengthened coupling beams support the use of bolted connections for the case of high seismic loading and displacement demands. In this study, a further experimental study on full-scale coupling beam specimens has been conducted to investigate the seismic behavior of strengthened RC coupling beams. The detailed effects of plate buckling and slip of shear connectors on the seismic behavior of strengthened coupling beams are presented. Furthermore, a theoretical study of plate strengthened coupling beams, taking into account the effect of partial interactions of the shear connectors, will be presented in the upcoming companion paper.

2. Experimental program

2.1 Specimens

A total of five RC coupling beam specimens with the same span-to-depth ratio ($l/h = 2.5$), dimensions, and details but with different strengthening schemes were fabricated and tested. Each of them was constructed to connect its ends to two RC panels (simulating part of the coupled shear walls) to investigate the behavior of beam-wall interactions. Two base beams were attached to the top and the bottom ends of each 90°-rotated specimen for fixing the specimen onto the loading frame through anchor-bolt connections.

The control specimen Unit CB1 was designed according to BS8110 (1985) to ensure that shear failure would occur prior to flexural failure. The specimen was identically reinforced in the wall piers and the base beams. These components were designed for the full loading capacity of a 500 kN hydraulic jack, which was the maximum possible load applied to the specimen during the tests, to ensure that they would not fail in the tests. The coupling beam was designed to achieve a loading of not more than 50 percent of the jack capacity so that the jack had enough capacity to load the strengthened coupling beams to fail. The compression and tension reinforcements in the coupling beam specimens were of two 20 mm diameter high yield deformed reinforcing bars. The dimensions and reinforcement details of the control specimen Unit CB1 are shown in Fig. 1. The coupling beams in the other four specimens (Units CB2 to CB5) were strengthened with bolted side steel plates with different plate thicknesses and shear connector arrangements to investigate their respective effects on the performances of the strengthened coupling beams. Unit CB4 has the same plate thickness as that of Unit CB2, but without shear connectors along the beam span. Unit CB5 has the same plate thickness as that of Unit CB3, but has a different number of shear connectors at the wall regions. While there are six shear connectors in Unit CB3, there are only four connectors in Unit CB5. All the steel plates used were 1250 mm long and 300 mm deep, matching the depth of
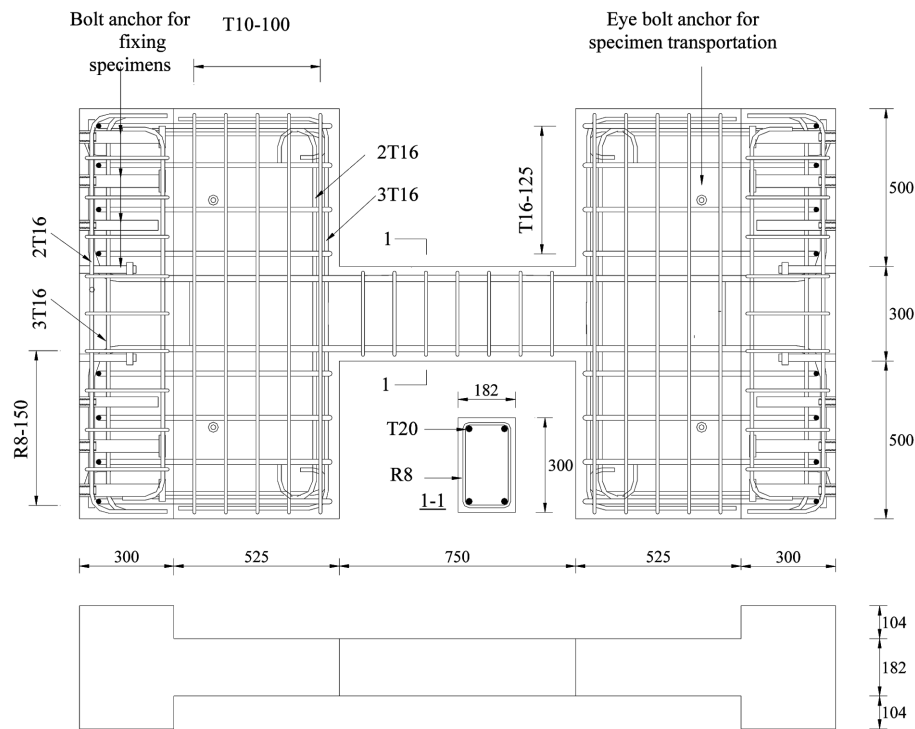
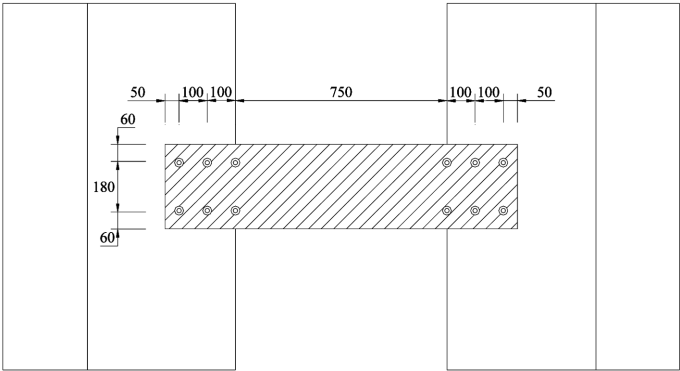Fig. 1 Reinforcement details and dimensions of Unit CB1

Fig. 2 Strengthening details of coupling beam in Unit CB4

the coupling beam. The four strengthened coupling beams required anchor sockets at specific locations for fixing the external plates. In order to simplify the fabrication, cast-in sockets were used in the test to form the mechanical connection system. Fig. 2 shows the detailed strengthening arrangement of specimen Unit CB4. Full details of the arrangements of the shear connectors at the steel plates for all the specimens are given in Fig. 3. The material properties of the concrete, steel plate, and reinforcement are given in Table 1.

The anchorage requirements at the ends of the steel plates were designed to transfer all the bending and shear forces from the steel plates to the wall anchors based on classical bolt group
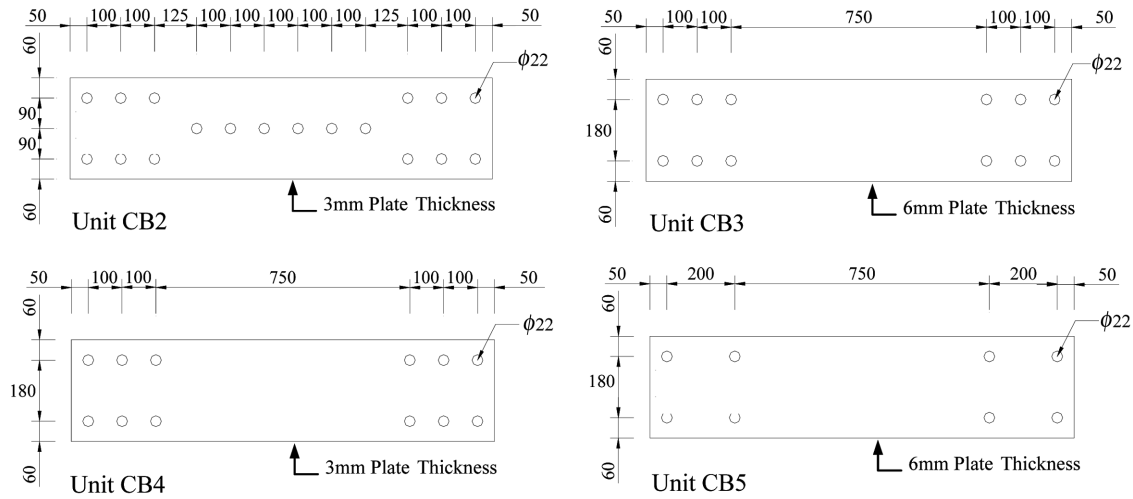
Fig. 3 Anchorage details of steel plates for the four specimens

Table 1 Material properties

Material		f_{cu} (MPa)	f_c' (MPa)
	Unit CB1	50.2	43.9
	Unit CB2	49.1	42.8
Concrete	Unit CB3	44.3	42.6
	Unit CB4	54.4	49.8
	Unit CB5	50.7	49.5
		f_y (MPa)	Young's Modulus (GPa)
	R8	462.7	212
	T10	571.0	211
Steel Bar	T12	529.3	207
	T16	549.2	210
	T20	504.1	203
Steel Plate	3 mm	326.0	190
	6 mm	337.2	186

theory. The number of shear connectors required depends on the bearing capacity of the concrete, the shear capacity of bolts, and the bearing and tearing capacities of the steel plate. All the bolts were designed to remain elastic at the ultimate loading stage. An anchor-bolt connection was chosen over an adhesive bonded construction for the following reasons:

1. The method of attachment is simple and reliable with no long-term problems of durability.
2. Adhesive bonded plates induce tensile-normal peeling stresses at the surface of the concrete along the edges of the plate. This imposes a severe limitation on the anchorage capacity of the plates. Shear connectors can be designed to transfer the designed force from the plate to the shear wall through the bearing of the cast-in bolts, allowing a much higher load-carrying capacity.

3. The failure of the section would become more ductile after plating, which is unlike bonded plates where tensile or peeling failure of concrete would cause brittle failure of the section.
4. Welding of multiple plates, if needed, can be achieved without damaging the epoxy adhesive, thus allowing for versatility of application.
5. No temporary supports are required while bolting.

For these connections, stress transfers between the plates and the concrete walls or beam must take place through the bolts. After the concrete had cured for 28 days, the external plates were fixed to the cast-in sockets with Grade 8.8 bolts of diameter 20 mm. Slightly larger clearance holes (22 mm in diameter) were provided in the steel plates for tolerances in fabrication. When all the bolts were fastened with a torque of 100 Nm to achieve a good connection between the bolt and the socket, the bolt heads were then welded to the plates. This arrangement could minimize any possible slippage amongst various components of the connection. It was found during the tests that failure of the weld connections at the bolt heads did occur under high reversed cyclic deformation demands for Units CB2 and CB3 and, hence, the weld size for Units CB4 and CB5 was re-examined and increased accordingly in order to be able to carry all the loads from the bolts.

2.2 Test set-up, instrumentation and loading program

The loading frame set-up designed by Kwan and Zhao (2002b), as shown in Fig. 4, was used for the tests. As revealed by the studies of Kwan and Zhao, realistic behaviors of the testing beams cannot be obtained due to the unparallel wall panels resulting from severe rotation during testing. In order to simulate the real situation in which the wall piers at the two ends of a coupling beam remain parallel under the deflection of the building, a parallel mechanism was installed to connect the upper rigid arm with the lower structural steel beam fixed on the floor. Loading was applied from a 500 kN actuator to the top end of each $90°$ rotated specimen through a rigid arm, with the line of action passing through the beam center. The bottom end of each specimen was attached to a horizontal structural steel beam that was fixed on a strong floor, while the top end was attached to a structural steel beam that could move horizontally during the loading process. In this way, the coupling beam was loaded with a constant shear force along the span, and a linearly varying bending moment with the point of contra-flexure at the mid-span.
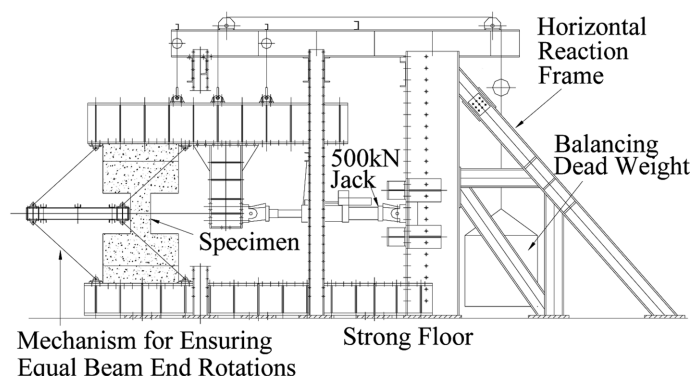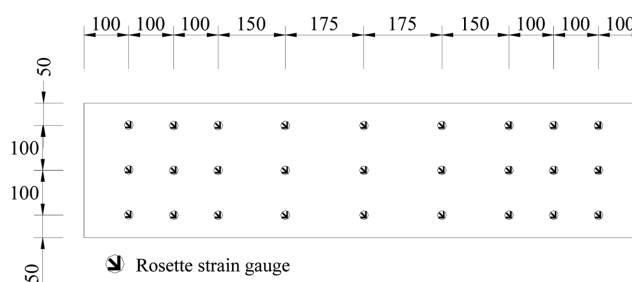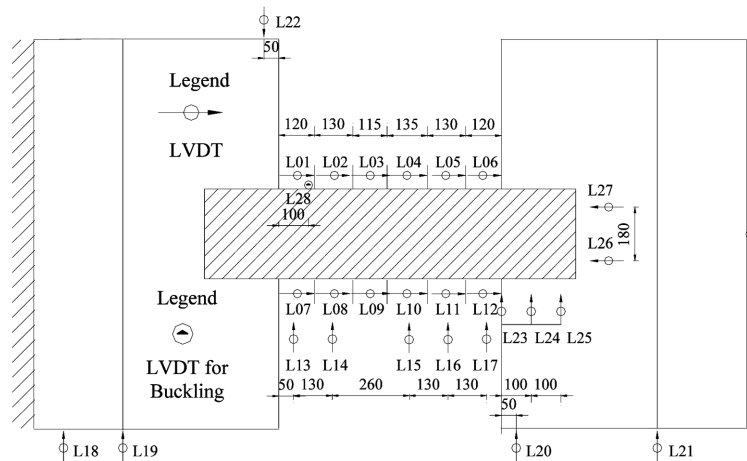

Fig. 4 Test-up – Reversed cyclic loading tests on specimens

Fig. 5 LVDTs arrangement for Units CB4 and CB5

Fig. 6 Rosette strain gauges arrangement for Units CB4 and CB5

A number of instruments, including Linear Variable Displacement Transducers (LVDTs) and strain gauges, were installed to the test specimens to study and monitor the behavior of the coupling beam during the loading process. Various strokes of LVDTs instruments (as shown in Fig. 5 for Units CB4 and CB5) were used to capture the deflection profile along the specimen axis perpendicular to the applied load, the curvature profile across the span of the coupling beam wall, the slips of shear connectors, and the local buckling deformation of the steel plate near beam-wall joint. Strain gauges were attached on the steel plates, the longitudinal bars, and the stirrups to investigate the deformations and internal load distributions of the steel plates and steel bars. Fig. 6 shows the rosette strain gauges of the steel plates for specimens Unit CB4 and Unit CB5.

The loading process was divided into two phases. The first phase was load-controlled and the second phase was displacement-controlled. Load-controlled cycles characterized themselves such that the termination of a cycle is based on a pre-assigned magnitude of shear force induced in the specimen. For displacement-controlled cycles, the termination of the cycle is based on the displacement of the specimen, which was measured by the LVDTs. As illustrated in Fig. 7, reversed cyclic loading was first applied to each specimen in a load-controlled cycle to up to 75% of the theoretical ultimate shear capacity (V_u^*) which was obtained by summing up the individual ultimate capacities of the RC beam and steel plates The strength of RC beam and steel plate were estimated by BS8110 (1985) and BS5950 (1990) respectively, and all the partial safety factors were taken as unity in the calculation. The subsequent cycles were displacement-controlled. The specimen was
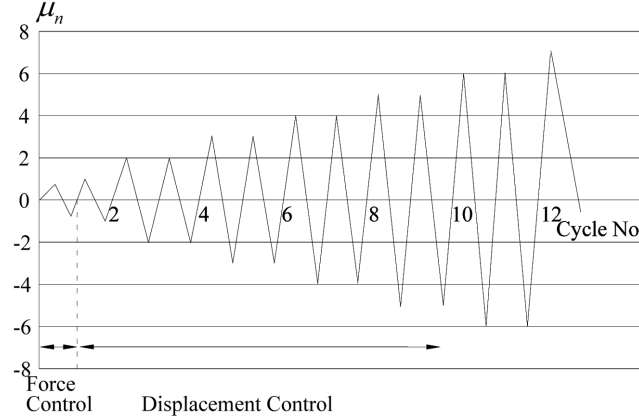
Fig. 7 Load program

displaced by a nominal ductility factor (μ_n) of 1 for one cycle, and then to each successive nominal ductility factor for two cycles to evaluate the strength degradation of the specimens. A chord rotation (θ) of the beams, defined as the differential displacement between the two beam ends in the loading direction divided by the clear span (l), were calculated using the measured displacements from the LVDTs. The nominal yield rotation (θ_{yn}) at $\mu_n = 1$ was obtained using the average of chord rotations corresponding to the positive and the negative loads at $0.75V_u^*$ in the first cycle divided by a factor of 0.75. The definition of the nominal chord rotation ductility factor is $\mu_n = \theta / \theta_{yn}$. In the third cycle and thereafter, the loading process continued to be displacement-controlled. The nominal ductility factor was increased, in accordance with Fig. 7. From the second ductility factor onward, repetition of cyclic loads was conducted at each ductility factor so that the evaluation of strength and stiffness degradation and retention was possible. The test was terminated when the peak load obtained in the first cycle of a nominal ductility level fell below the lesser of $0.8V_u^*$ and $0.8V_{max}$, where V_{max} is the measured ultimate shear capacity. The test specimen was then considered to have failed.

3. Experimental results

3.1 Strength and ductility

The performance of the specimens was evaluated through the measured strains and LVDT data as well as the observed damage and crack patterns. Several parameters are defined to interpret the results of the tests. The ultimate rotation θ_u is defined as the chord rotation angle at $0.80V_u^*$ of an envelope curve on the softening branch when the strength drops to 20% of the theoretical strength, and the yield chord rotation angle θ_y is defined by an equivalent bilinear response curve that provides an equal area to that of the envelope curve of specimen. The maximum ductility factor i is equal to dividing the ultimate rotation θ_u by the yield rotation θ_y. The initial stiffness, K_0, is equal to dividing the ultimate load by the yield chord rotation. For more details, one can refer to Fig. 8 for the definitions of the parameters. Values of the maximum nominal ductility factors, μ_n, and maximum ductility factors, μ, of the five specimens are shown in Table 2.
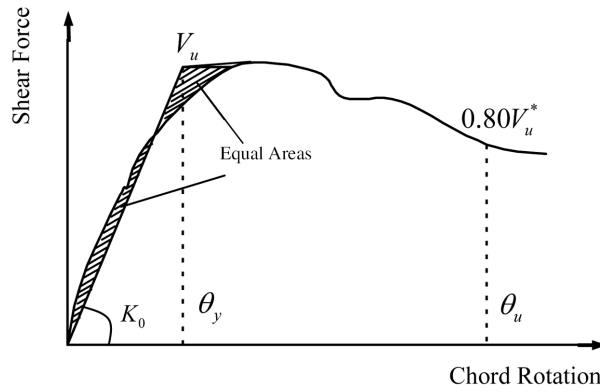
Fig. 8 Definitions of parameters

Table 2 Summary of experimental results

Unit	V_u^* (kN)	V_{max} (kN)	K_o (kN/mm)	θ_{yn} (rad)	θ_y (rad)	θ_u (rad)	μ_n	μ
CB1	151	213	37.9	0.0048	0.0078	0.0297	6.2	4.0
CB2	232	291	40.0	0.0072	0.0095	0.0365	5.1	3.8
CB3	274	363	36.6	0.0095	0.0129	0.0482	5.1	3.7
CB4	232	354	41.3	0.0072	0.0117	0.0360	5.0	3.1
CB5	274	418	35.1	0.0094	0.0158	0.0560	7.1	3.6

The attached plates increased both the ultimate capacity and deformability of the specimen beams, Unit CB2 to CB5. Compared with the values for Unit CB1, the ultimate shear (V_u) and the ultimate measured chord rotation angle (θ_u) of Unit CB2 were increased by 37% and 23% respectively, however, the ultimate shear and the ultimate measured chord rotation angle of Unit CB4 were increased by 66% and 22%, respectively. The difference between the ultimate strength of Unit CB2 and Unit CB4 is due to the presence of a row of shear connectors along the beam span of Unit CB2 and the immature tearing failure of some welds in Unit CB2. For the ultimate shear and the ultimate measured chord rotation angle of Unit CB3, the values were increased by 70% and 62% respectively, and for those values of Unit CB5, they were increased by 96% and 90% respectively. Although Unit CB5 has a smaller number of bolt connections in the end of the steel plates, the ultimate strength and deformation of Unit CB5 is larger than that of Unit CB3 as there was no immature tearing failure of welds, and because of the subsequent excessive bolt slips in Unit CB5 during the test when the specimen reached its ultimate capacity.

It was found, from Table 2, that attaching steel plates to beams would slightly reduce the ductility of the coupling beams. As the increase in the yield chord rotation (θ_y) was slightly larger than that of the ultimate measured chord rotation angle (θ_u), The maximum ductility factor (defined as θ_u/θ_y) was therefore slightly reduced for the strengthened beams. On the other hand, coupling beams strengthened with bolted side plates can enhance the yield rotation angle. The initial stiffnesses K_0 for Units CB1 to CB5 are shown in Table 2. It was also noticed that the maximum increase of stiffness among the strengthened specimens is only about 9%. Since a smaller increase in stiffness induces a smaller increase in absorbing forces in a coupling beam during an earthquake, it is a

desirable feature for plate-strengthened coupling beams to resist seismic induced internal forces. Comparing the strength and ultimate deformation of the strengthened coupling beam with those of the control specimen, it can be concluded that attached steel plates can significantly increase both the strength and deformation capacity of the beams with little increase in the initial stiffness.

3.2 Load-rotation curves

Fig. 9 shows the applied shear force against the chord rotation for all the specimens. It can be seen, after comparing with the control specimen, that the strength and deformation capacity in terms of chord rotation of all the plate-strengthened coupling beams were increased. The shear force – chord rotation curve of the control specimen (Unit CB1) exhibits substantial pinching, especially at large deflection amplitudes. Such pinching leads to rapid stiffness degradation and less energy dissipation. While Units CB2 to CB5 underwent less serious pinching than Unit CB1 due to strengthening of the steel plates, Unit CB2 and Unit CB3 behaved, respectively, in a manner similar to Unit CB4 and Unit CB5, as they were strengthened with the same thickness of steel plates. However, the shear force – chord rotation curves of Units CB3 and CB5 have less pinching than
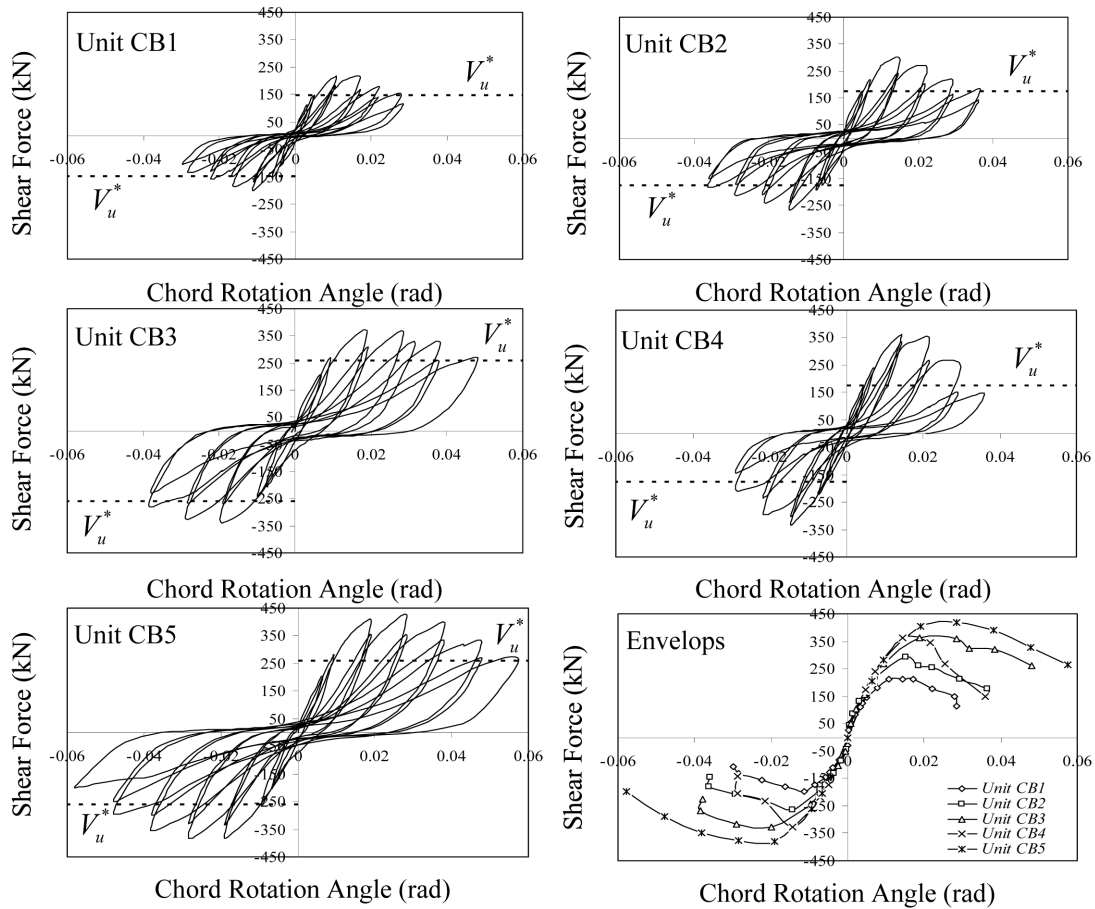

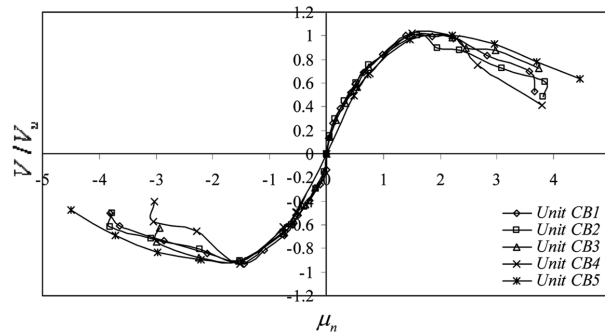Fig. 9 Load-chord rotation hysteresis loops and envelope curves

Fig. 10 Normalized load-chord rotation envelope curves

those of Units CB2 and CB4 due to less serious buckling of the thicker steel plates, as observed in the tests.

It can be seen from the envelope curves in Fig. 9 that all the specimens have the same behaviors before the applied loads reached the yield loading of Unit CB1. In this early stage, the rotation of the coupling beam was small and the steel plates had not been activated due to the small internal movements between the bolt shanks and the cast-in anchors. In general, the reinforced concrete part of the coupling beams carried nearly all of the loads. As the applied load increased, the chord rotation increased and the concrete cracked under tension. The load-resisting action of the steel plates was gradually increased through the activation of the bolt connections. As the deformation demand increased, with the concrete crushing and the steel plates yielding in tension areas (for thick steel plates) or buckling in compression areas (for thin steel plates), the strengthened beams reached their ultimate loads. When the specimens underwent further load cycles, more the concrete cracks and crushing became more serious, and the steel plate yielding and buckling became more severe. The failure of the concrete section led to failure of the composite beams.

The envelopes of the normalized load versus ductility factor are shown in Fig. 10 to illustrate the responses of the specimens under monotonic increasing loads. Normalized curves were used to eliminate the pre-existing difference of the strengthening schemes and material properties. There was not much difference in the behavior among the specimens before they reached their ultimate loads (i.e., when $V/V_{max} = 1$). This revealed that the difference of the strengthening scheme was mainly displayed in the post-peak stage.

3.3 Strength and stiffness degradation

The strength degradation in repeated cycles are shown in Fig. 11 in terms of the comparison of the peak loads of each specimen at a nominal ductility level (V_{peak1}) and in the repeated loading cycles (V_{peak2}). As a control specimen, Unit CB1 experienced the strength degradation from 13% to 25% in the repeated loading cycles. This was mainly due to the formation of cracks and crushing of concrete in the coupling beam during loading cycles. Unit CB2 had a larger strength degradation (nearly 18%) than other specimens after undergoing the first inelastic cycle. This was probably due to the formation of plenty of concrete cracks, which were distributed across the whole coupling beam span and resulted from the effects of the cast-in anchor-bolts along the span. Although the shear connectors at the beam span can help to transfer forces and partially prevent local buckling of the steel plates, these connectors may weaken the concrete in critical sections of the beam span,
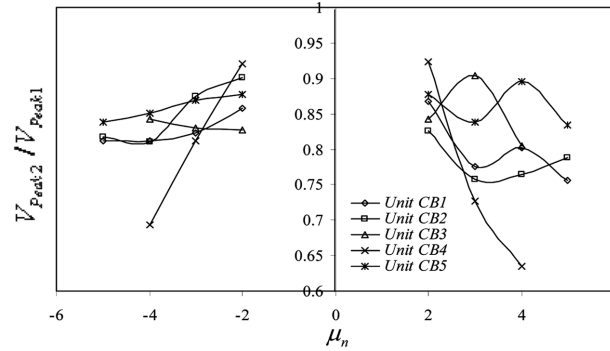
Fig. 11 Retentions of load capacities of specimens in repeated cycles

such as near the beam-wall joint, and, thus, the strength retention of the coupling beam. In the latter sections, the crack pattern and the stirrup strains of Unit CB2 will demonstrate this effect. In the negative half of the loading cycles, the peak load is generally lower than that of the positive half, and the difference between $-V_{peak1}$ and $-V_{peak2}$ is smaller. From Fig. 11, it can be observed that the strength retention of Unit CB2 in the negative half loading cycle was better than that in the positive half. After the first inelastic cycle, the strength degradation of Unit CB3 (nearly 16%) was larger than that of the control specimen Unit CB1. The difference in the strength degradation is due to a faster deterioration of the concrete caused by a higher axial force interaction from the thick (6 mm) steel plate, and the reduced contribution from the steel plates which were attributed to damage of the welds at some of the shear connectors. Although Unit CB4 was strengthened with 3 mm thick steel plates without shear connectors along the beam span, it had smaller strength degradation (nearly 7%) than other specimens after undergoing the first inelastic cycle, and experienced larger and faster strength degradation than any other Units in the subsequent loading cycles. This undesirable situation is probably due to buckling of the steel plates at the beam-wall joints in addition to the loss in concrete strength as the increase of the rotation demands. The performance of the strength retention in Unit CB5 is the most desirable. It almost kept the same strength retention capacity (nearly 85%) in all the loading cycles. This indicates that steel plates could undertake part of the concrete load lost in the coupling beam as the increase of the beam rotations. Unit CB5 was strengthened with 6 mm thick steel plates. As the local buckling was not serious, it had little effect
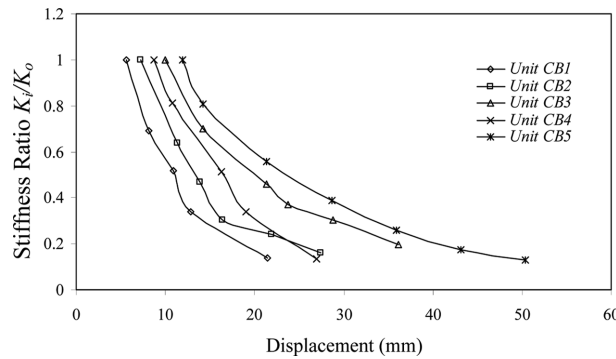

Fig. 12 Degradation of stiffness

on the load-carrying capacity of the beam. Therefore, it can be concluded that shear connectors between concrete and steel plates as well as local buckling of steel plates play an important role in retaining the strength of a medium-length strengthened coupling beam under inelastic deformations.

The degradation of the stiffness for all the specimens are analyzed and shown in Fig. 12. In the figure, the initial stiffness K_0 is defined as the ultimate shear force divided by the yield displacement, and K_i is the instantaneous secant stiffness at a certain displacement. The stiffnesses at loading peaks of the first positive half circle for each nominal ductility factor were calculated. The ratios K_0/K_i, which are higher than the yield displacements for all the specimens, are shown in Fig. 12. The initial stiffnesses K_0 of Units CB1 to CB5 are 37.9 kN/mm, 40.0 kN/mm, 36.6 kN/mm, 41.3 kN/mm and 35.1 kN/mm respectively. Although Units CB2 and CB4 were strengthened with thinner steel plates (3 mm), they have slightly higher initial stiffnesses than that of the control specimen Unit CB1. This is mainly due to the increment of the nominal yield displacement not being proportional to that of the ultimate shear force. However, the initial stiffnesses of Units CB3 and CB5, which were strengthened with thicker steel plates (6 mm), are slightly lower than that of specimen Unit CB1. This means that strengthening specimens (Units CB3 and CB5) not only resulted in an increase in their strengths, but also in an increase in the yield displacements. All these features are desirable in the aseismic retrofitting of RC structures. Comparing the stiffness degradation of Units CB2 and CB4, it is noticed that the stiffness of Unit CB2 decreased faster than that of Unit CB4 in the final two nominal ductility factors. Unit CB3 and Unit CB5 had almost identical stiffness degradation trends, but Unit CB5 experienced more displacement. From Fig. 12, it can be further observed that all the strengthened coupling beams have lower stiffness degradation rates and a higher displacement capacity than those of the conventionally reinforced Unit CB1.

3.4 Energy dissipation

Energy dissipation capacity is another important factor in the evaluation of the seismic performance of RC coupling beams. Herein, the energy dissipated (W_d) in each half cycle is evaluated. The relationships between the cumulative energy dissipation and the cumulative displacement in all the loading cycles for each specimen are determined (see Fig. 13). Comparing the energy dissipation values of Units CB2 to CB5, it can be observed that the beams strengthened with thicker steel plates (Units CB3 and CB5) dissipate more energy than that of Unit CB2 with thinner steel plates. The difference in energy dissipation is due to the fact that the ductile steel
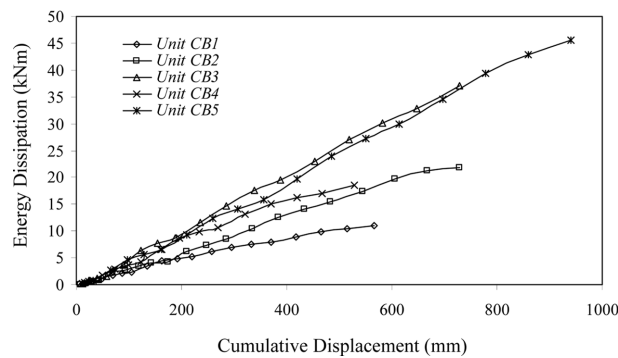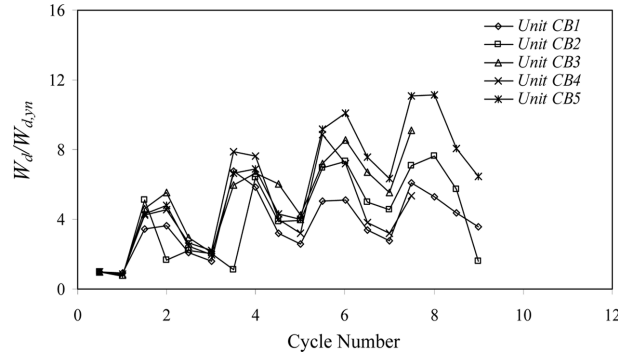

Fig. 13 Energy dissipation

Fig. 14 Normalized energy dissipated

plates possess better deformability and higher energy dissipation via inelastic deformation, and this deformation resists most of the applied load as the ductility factor increases. The cumulative energy dissipation of Unit CB4 being higher than that of Unit CB2 again demonstrates that shear connectors installed at the beam span has detrimental effects on coupling beams. Units CB3 and CB5 have similar cumulative energy dissipation trends. However, due to better workmanship of the weld connection at the shear connectors, Unit CB5 dissipated more energy. Although there are some differences in the behaviors of Units CB2 to CB5 in the tests, all the strengthened coupling beams exhibit significant improvement in the inelastic behaviors in terms of higher energy dissipations.

Fig. 14 shows the energy dissipated W_d normalized by the energy dissipated in the positive half cycle at nominal yield ($W_{d,yn}$). At each nominal ductility level, all the beams, except Unit CB2, dissipate a larger amount of energy in the first loading cycle than the second repeated cycle, and energy dissipated in the negative half-cycle was generally slightly larger than that in the positive half-cycle. The amount of energy dissipation dropped in the repeated cycle was probably due to the extension of slip at shear connectors and damage of concrete with both effects occurring in the early cycles. During the positive half cycle of the second cycle ($\mu_n = 2$), W_d in Unit CB2 increased the most rapidly among all specimens. However, in the subsequent negative half cycle, W_d decreased rapidly back to a value near $W_{d,yn}$. Even in the successive third cycle (second loading cycle of nominal ductility 2) and the positive half cycle of the fourth cycle ($\mu_n = 3$), W_d had no significant increment. This indicates that the concrete in the beam was seriously damaged in the positive half cycle of the second cycle. After the sixth cycle, the increment of the energy dissipation W_d in Unit CB4 was lower than that in Unit CB2, due to buckling of the steel plates as well as damage to the concrete which reduced its strength and energy dissipation ability; tests on Unit CB4 were terminated after the seventh cycle. It was noticed that Units CB3 and CB4 had better cumulative energy dissipations during loading cycles. However, due to the effectiveness of the shear connectors and less buckling of the steel plates throughout the test, Unit CB5 exhibited the best performance in terms of the normalized energy dissipation.

3.5 Crack and damage patterns

The crack patterns in the wall piers of all the specimens were similar. The wall piers, including the joint regions, only experienced slight damage when the beams failed. Fig. 15 shows the crack patterns at failure for strengthened coupling beams. The external plates had been taken away to
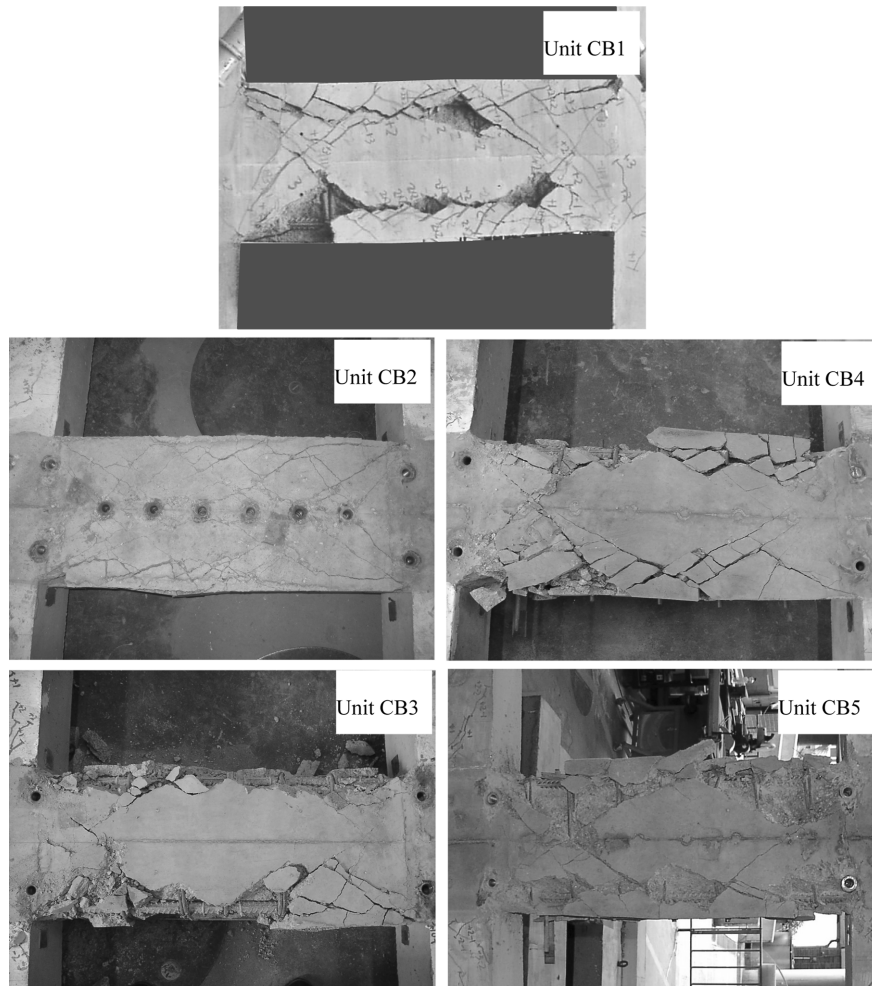
Fig. 15 Specimens at failure

examine the crack patterns of concrete along the span of the strengthened beams. For Unit CB2, cracks were evenly distributed along the span of the beam and spalling of concrete along the longitudinal reinforcement was observed. However, no significant plastic hinge could be found. The row of bolts along the span of the coupling beam could partially prevent local buckling of the thin steel plate (3 mm) but, at the same time, they led to serious concrete damage at the failure stage. Therefore, in common engineering practice, it is not recommended to provide shear connectors at the span to prevent local buckling of thin steel plates. Thicker steel plates or other means, such as stiffeners, should be used instead to avoid local buckling. For Unit CB3 with 6 mm steel plates, plastic hinges formed at the ends of the beam were observed. The thick steel plate can effectively mitigate buckling of the plate. As the ductility factor increased, the concrete cover to the main reinforcement gradually spalled off due to the increasing compressive force developed along the beam. Serious crushing of concrete under compression was observed and led to the ultimate failure of the beam. For Unit CB4, plastic hinges were formed at the ends of the beam. The core concrete in the centre part of the beam has apparent cracks. As the ductility factor increased, the concrete

cover also gradually cracked and spalled off due to the increasing tensile and compressive force developed along the beam. Upon comparing Unit CB2 with Unit CB4 in the beam spans, significant differences in the crack patterns could be observed due to different arrangements of shear connectors. The buckling of steel plates, formation of plastic hinges, and the serious crushing of concrete under compression led to the ultimate failure of the coupling beam of Unit CB4. For Unit CB5, the concrete cover was seriously damaged, and stirrup bars could even be observed from the side faces of the beam. Longer plastic hinges were formed at the ends of the coupling beam. Only a small rhombic area of core concrete in the central part of the beam was observed to be without obvious cracks. Since Unit CB5 experienced larger loads and deformation, together with the formation of longer plastic hinges and more intensive cracks, serious spalling of concrete was found which resulted in the final failure of the specimen.

3.6 Curvature profiles

Six pairs of LVDTs (as shown in Fig. 5) were installed at the top and bottom faces of each specimen to monitor the deformation during the loading process. The readings obtained were then converted to values that represented the average curvature values of the sections by simply dividing the difference of the readings between two LVDTs on the same horizontal level with the horizontal spacing and the vertical spacing between the adjacent LVDTs. For an easier visualization, the curvature profiles of the specimens with the nominal ductility factors +1, +2 and +3 were plotted in Fig. 16 before the data became unreliable at some locations, resulting from cracks or the crushing of concrete across the LVDTs. A positive curvature indicated that the section was under a hogging moment, i.e., the top and bottom fibres were in tension and in compression, respectively.

The variations of the curvature with the span length of the coupling beams are shown in the left hand side of Fig. 16. The x-axis of the graph represents the distance from the mid-span of the coupling beam and the y-axis represents the curvature of the coupling beam. The theoretical yield curvature of about 0.029 rad/m in Unit CB1 was exceeded near the beam-wall interfaces in all the specimens at the peak of the nominal ductility factor 1. This observation reflected that the inelastic deformation had begun in all the specimens at this stage. The increments in the curvature were associated with cycles of a greater ductility factor. Towards the later stage of loading, the damage of the concrete and buckling of the steel plates contributed to the accelerated rate of increase in the curvature in the plastic hinge region. The substantial increase in curvatures at nominal ductility factors of 2 and 3 showed that the plastic hinges had undergone considerable rotations, mainly in the region with a length of about 0.5 to 1.5 times the depth of beam section. For example, it was found that for specimen Unit CB1, the curvature values within a distance of about 155 mm from the beam-wall interface exceeded the effective yield curvature. The region was thought to have worked as a hinge which contributed to a substantial portion of the deformations of the specimens. However, the increase of the curvature in Unit CB1 is more drastic than those in other Units at a ductility factor +3. This shows that conventionally reinforced coupling beams, without retrofitting with bolted side steel plates, are more brittle, as excessive displacement can cause serious spalling of concrete in compression areas which leads to sudden failure of the structural member. For other specimens, it was observed that the specimens with thicker steel plates (Unit CB3 and Unit CB5) could sustain higher curvatures when compared with those of Units CB2 and CB4. Therefore, it can be concluded that specimens with thinner steel plates are prone to buckling and cannot promote a high deformability.
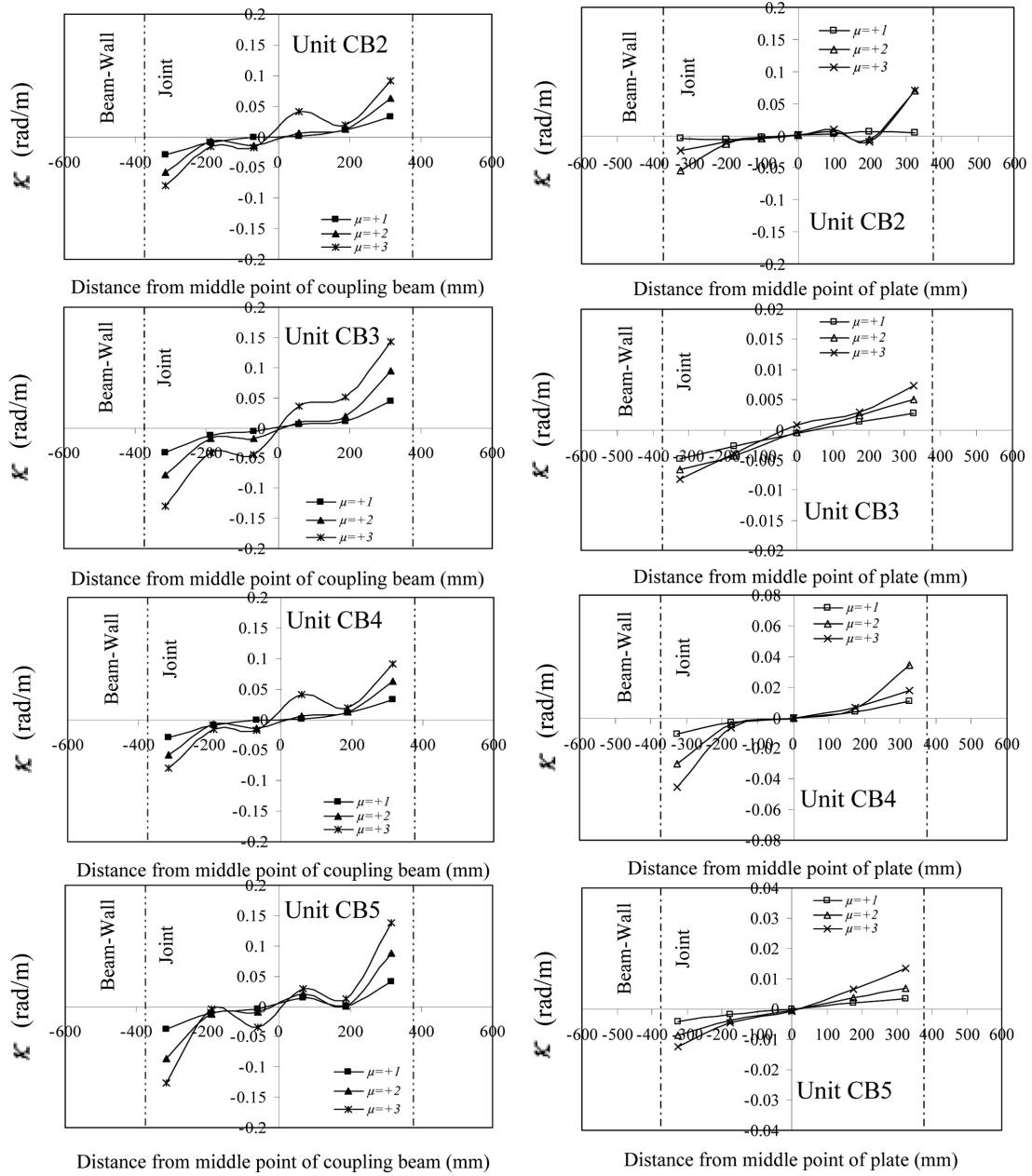
Fig. 16 Curvature profiles of RC coupling beams and steel plates

3.7 Behavior of steel plates

The stress, strain and internal force distributions of the external steel plates can be determined by analyzing the data obtained from the rosette strain gauges attached to the plate surfaces, as well as observing the macro-deformations of the steel plates. The shear and axial strains of the steel plates are first calculated from the measured strains. Then, by assuming a linear variation of the strains
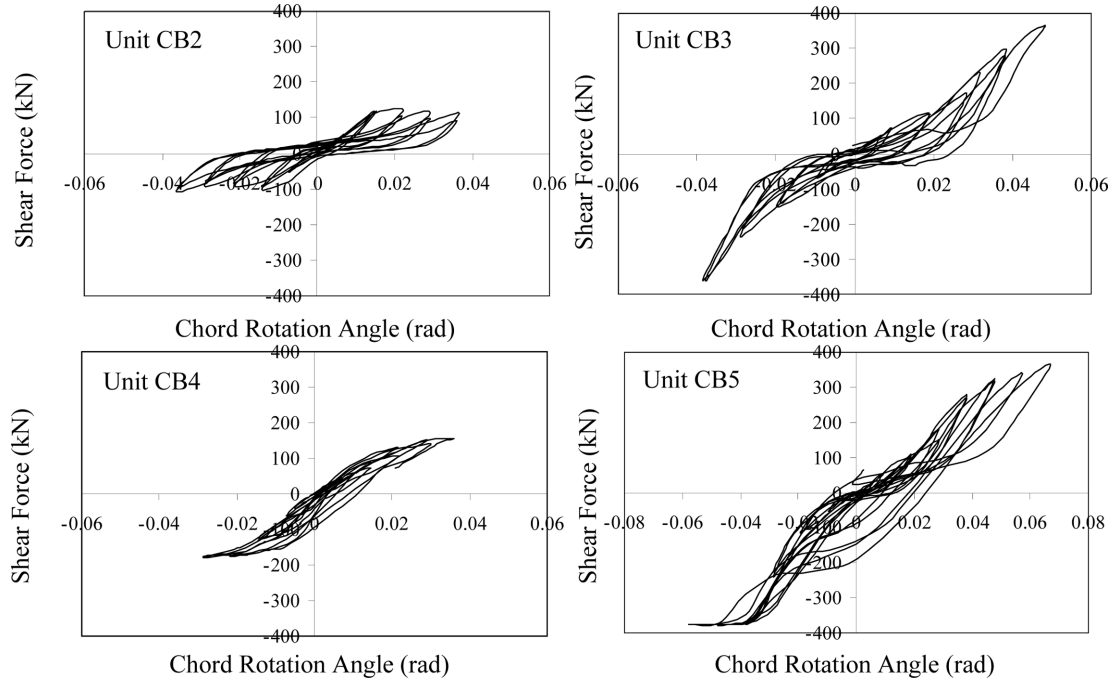
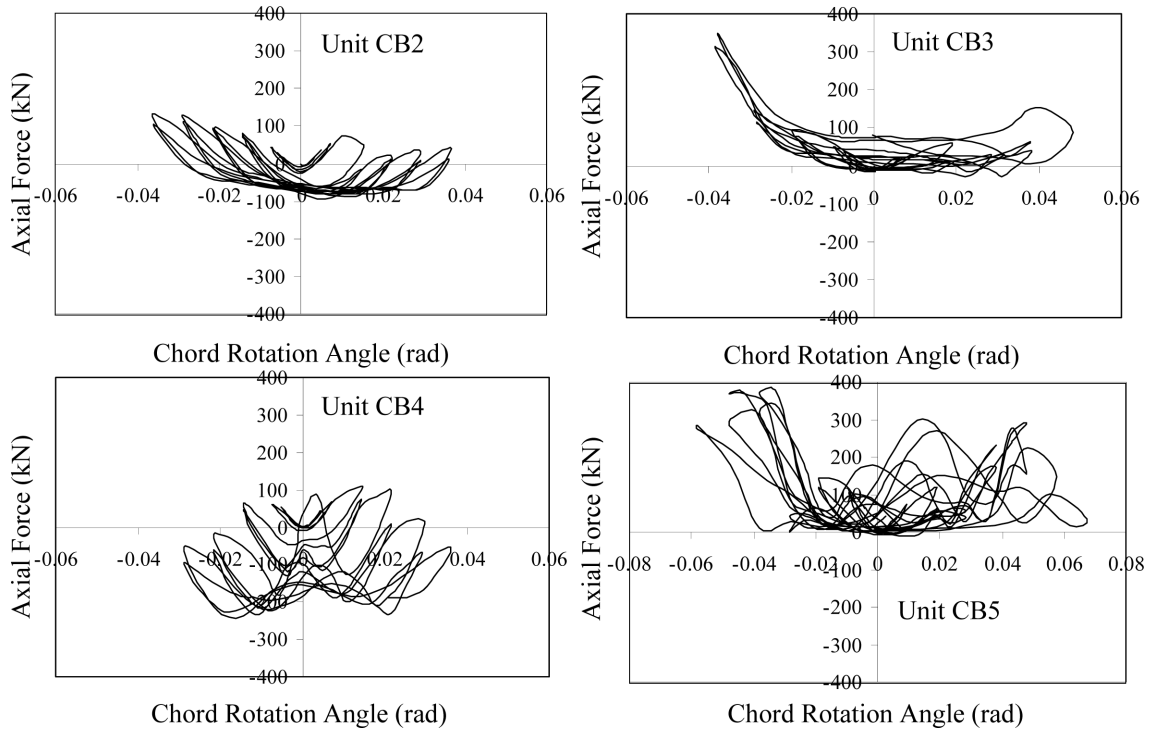Fig. 17 Plate shear forces against chord rotation angle

Fig. 18 Plate axial forces against chord rotation angle

between the strain gauges and invoking the stress-strain relationship of steel, the internal forces at each section can be calculated accordingly. Fig. 17 and Fig. 18 show the variations of the internal shear forces and internal axial forces at mid-span of the external steel plates, respectively. The results reveal that the steel plates for all the specimens took up more shear loads as the beam rotation increased (shown in Fig. 17). The plates sustained almost all the shear loads when the nominal ductility factor was higher than 3.

In Unit CB2, the shear resistance of the steel plate reached its maximum capacity when the nominal ductility factor reached +2. This is because local yielding and buckling of the steel plate had occurred and limited its load-carrying capacity. Owing to elongation of the concrete beam under cyclic loads and the composite effect between steel plates and reinforced concrete, tensile forces were developed in the steel plate when the loads were approaching the peak load at each positive and negative cycle. When the tensile stress induced in the steel plate had reached its yield stress (after a nominal ductility factor +2), permanent plastic deformation occurred and caused an extension of the steel plate. As a result, the span length of the steel plate was longer than that of the reinforced concrete counterpart under the next reverse cycle. When the chord rotation angle was reduced to zero, the strain compatibility between the reinforced concrete and the steel plate resulted in the compression developed in the steel plate and tension induced in the reinforced concrete. So there was a negative value of the axial force, as is shown in Unit CB2 of Fig. 18. In Unit CB3, the shear force experienced by the steel plates increased with the nominal ductility factor, whereas the axial force variation was not stable due to immature tearing of some of the weld connections between the bolts and the steel plate. As a result, the energy dissipated by the steel plate in Unit CB3 was lower than that of Unit CB2. Due to the elongation of the RC beam of Unit CB3, the composite effect between steel plates, and the RC beam as well as slight local plastic deformation of the 6mm steel plates, there was a positive value of an axial force in the steel plates after the nominal ductility factor +2. In Unit CB4, the hysteretic relationship of shear force of the steel plates with chord rotation was different from that of Unit CB2. The main reason is that more serious local buckling and even global buckling of the steel plates in Unit CB4 had occurred. However, the steel plates in Unit CB4 attained a larger shear force than that in Unit CB2 due to better shear connection in Unit CB4. The axial force of the steel plates in Unit CB4 was also unstable due to buckling deformation after a nominal ductility factor of +2. In Unit CB5, the steel plates attaining the highest shear force and having larger permanent deformation after the first inelastic deformation cycle (μ_n = +2) are shown in Fig. 17. The axial force in the steel plates in Unit CB5 which was, in fact,
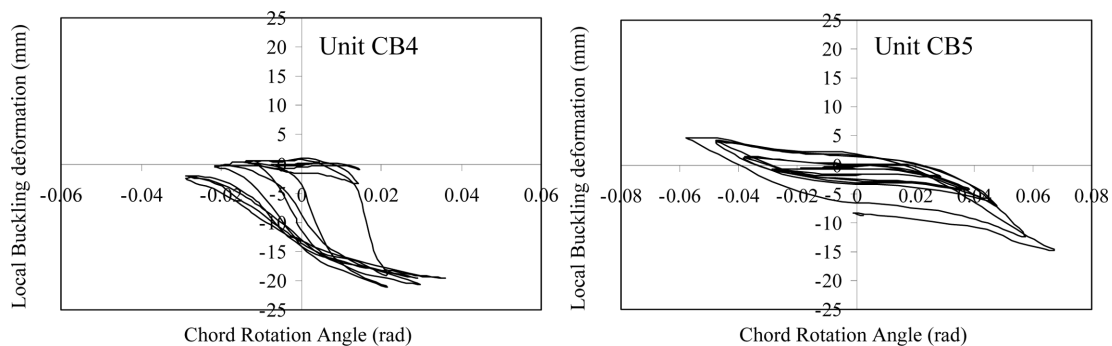

Fig. 19 Local buckling deformation of steel plate against chord rotation angle

unstable (as observed from Fig. 18) was mainly due to the large inelastic deformation in the steel plates.

During the test, the external steel plates took up the combined bending, shear and axial forces. The induced diagonal compressive forces caused a local buckling instability of the steel plate when the applied loads were greater than the critical limit. This local buckling phenomenon is known as the unilateral constraint buckling problem and is critical for externally bolted side plate strengthened coupling beams under reversed cyclic loads. One LVDT had been installed to monitor local buckling of the steel plate near the beam-wall joints in Unit CB4 and Unit CB5 (as shown in Fig. 5). Fig. 19 shows the variations of the local buckling deformation of the steel plates with chord rotation of the coupling beams. It is observed that the local buckling was more severe in Unit CB4 than in Unit CB5 after a nominal ductility factor +1 due to the use of thin (3 mm) steel plates. In spite of the buckling of the steel plates, no significant loss in strength was found in Units CB2 to CB5 just after plate buckling.
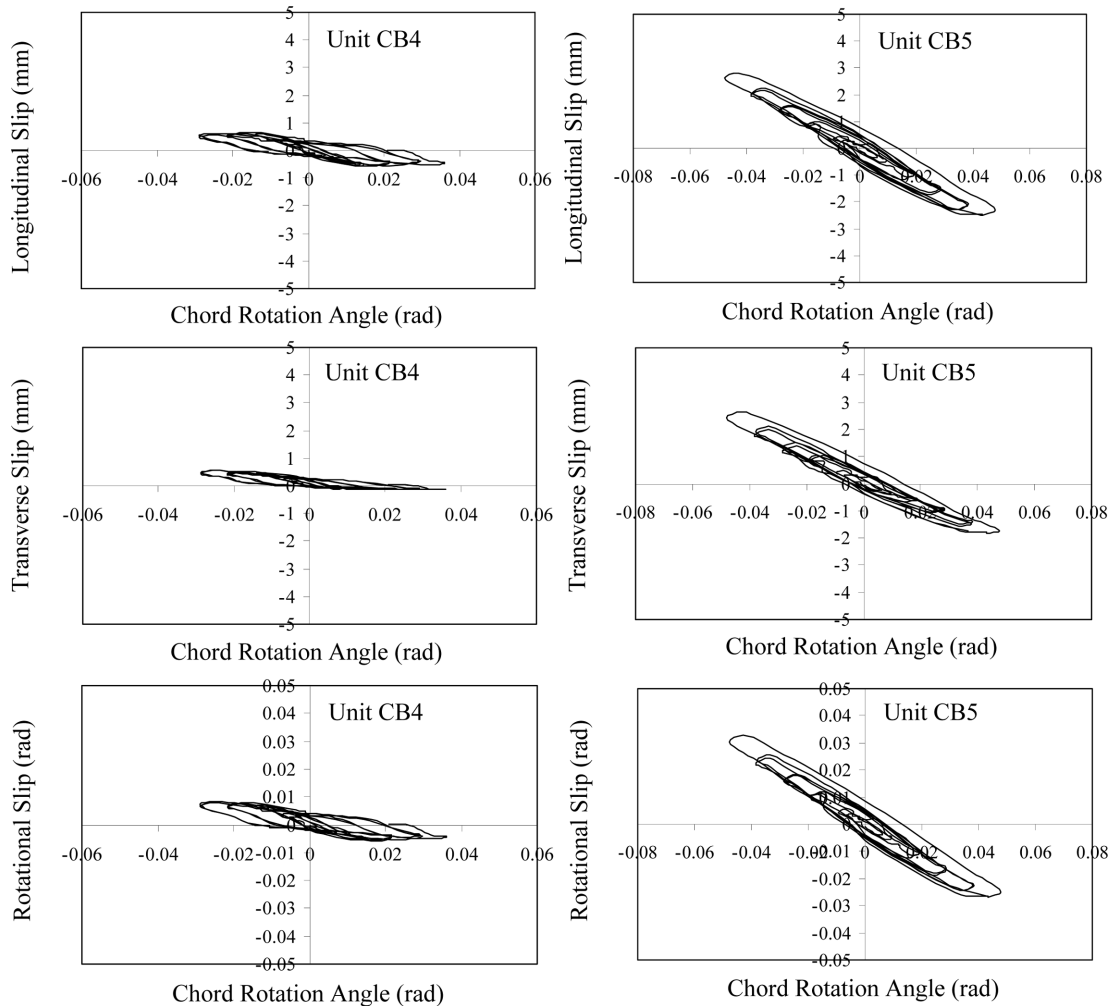

Fig. 20 Bolt group slip against chord rotation angle

3.8 Slip of shear connectors

The composite effect of a bolted side plated reinforced concrete coupling beam is achieved with the mechanical action of anchor bolts. The bolts resist the interface shear by mechanical action and therefore they must slip, and the maximum slip strain occurs at the position of maximum moment. Furthermore, the slip of composite bolted side plated reinforced concrete coupling beam differs substantially from the behavior of standard composite steel and concrete beams (Oehlers and Bradford 1995, Ohelers and Bradford 1999). This is because the latter is only subject to longitudinal slip, whereas, the former is subject to both translational and rotational slips. Five LVDTs had been installed in Unit CB4 and Unit CB5 (as shown in Fig. 5) to evaluate the slips of the bolt groups at the wall regions during the tests.

The average longitudinal, vertical and rotational slips of the anchor-bolt group were calculated and are plotted in Fig. 20. It can be observed that the transverse slips are less than the longitudinal slips in these two specimens, which is consistent with the previous results that the shear forces are less than the axial forces of the steel plates. In Unit CB4, the longitudinal, transverse and rotational slips remained constant after the first inelastic cycle (μ_n = +2). This was probably not due to yielding of shear connectors, but resulted from buckling of the steel plates which was unable to sustain the increasing internal force from the steel plates. For Unit CB5, the longitudinal, transverse and rotational slips kept increasing as the inelastic cycles progressed, and they increased almost linearly with the chord rotation of the specimen. This indicates that the steel plates had sustained more loads as the ductility cycle increased and the shear connectors remained linearly elastic. The maximum longitudinal slips of Unit CB4 and Unit CB5 were 0.65 mm and 2.81 mm respectively. The maximum transverse slip of Unit CB4 was 0.54mm and that of Unit CB5 was 264 mm. The rotational slip was smallest among longitudinal, transverse and rotational slips. The maximum rotational slip of Unit CB4 was 0.008 rad and that of Unit CB5 was 0.032 rad.

4. Conclusions

The performances of five medium-length coupling beams, which include one reference conventionally reinforced concrete (RC) coupling beam and four strengthened coupling beams with bolted side plates, tested under reversed cyclic loads, have been presented in this paper. The experimental findings for these strengthened coupling beams with medium span/depth ratios are summarized as follows:

1. *General behavior*: It is found that the conventionally reinforced coupling beam without retrofitting with bolted side steel plates is more brittle. In contrast, the attachment of an external steel plate by bolted connections can considerably enhance the strength, deformation capacity, and energy dissipation as well as reduce the stiffness degradation rate and slightly increase the initial stiffness of RC coupling beams under reversed cyclic loads.

2. *The Hierarchy of Failure*: The sequence of failures are as follows: concrete, steel plate, and then the shear connectors. At the early stages, damage at the concrete accounts for the major part of the strength loss. At the later stages, steel plates undertake part of the concrete load lost, and yielding and buckling of the steel plates as well as slippage or damage of shear connectors may contribute as another source of strength degradation.

3. *Effect of Plate Buckling*: The experimental study revealed that buckling of steel plate always

occurs after the concrete reaches its ultimate capacity. After plate buckling, the compressive force originally taken up by the steel plate is transferred to the concrete. Provided that concrete can have the reserved capacity to take up the additional compressive load, detrimental effects due to plate buckling on the beams will be relatively small. Conversely, if concrete is already highly loaded, the additional compressive force from the steel plate will accelerate the rate of deterioration of the concrete and significantly affect the post-peak behavior of plate-strengthened beams. Comparing the energy dissipation values, it can be observed that the beams strengthened with thicker steel plates (Units CB3 and CB5) dissipate more energy than those with thinner steel plates (Units CB2 and CB4). The difference is mainly due to the fact that thicker steel plate can avoid local buckling and pinching in the load-deformation curve. The ductile steel plates possess a better deformability and higher energy dissipation via inelastic deformation. The performance of the beams (Units CB2 and CB4) using a thin steel plate is not satisfactory as their strength retention is poor after the peak load due to serious local buckling of the plates near the beam-wall joints.

4. *Effect of the Arrangements of Shear Connectors*: Shear connectors play an important role in retaining the strength of a medium-length strengthened coupling beam under inelastic deformations. Although adding shear connectors at the span (for Unit CB2) can partially prevent local buckling of the thin steel plate, it is not recommended that they be used in general practices. This is because an additional load transferred to concrete can cause serious damage to the beam span, as observed in the test. Thicker steel plates (e.g. Unit CB5) or other means, such as adding stiffeners, should be used to avoid local buckling. Due to insufficient leg length of the fillet welds at some of the shear connectors (Units CB2 and CB3), premature failures of the welds were observed during the test in the post-peak stage. It is obvious that proper arrangement and good quality workmanship in the installation of shear connectors are of the utmost important to ascertain the proper performance of the strengthened beams.

5. *Effect of Slip of Shear Connectors*: It is found that the curvatures of steel plates are generally smaller than those of the RC counterparts in the corresponding specimen. This disparity in curvatures indicates that translational and rotational partial interactions between steel plates and the RC beam weakened the load-carrying capacity of the steel plates in the coupling beams. Further theoretical study of plate strengthened coupling beams, taking into account the effect of partial interactions, will be presented in the upcoming companion paper.

Acknowledgements

References

Ahmed, M., Oehlers, D.J. and Bradford, M.A. (2000), "Retrofitting reinforced concrete beams by bolting steel plates to their sides, Part 1: Behavior and experiments", *Struct. Eng. Mech.*, **10**(3), 211-226.

Barnes, B.A., Baglin, P.S., Mays, G.C. and Subedi, N.K. (2001), "External steel plate systems for the shear strengthening of reinforced concrete beams", *Eng. Struct.*, **23**, 1162-1176.

BSI (1985), "BS8110 Part 1: Code of practice for design and construction, structural use of concrete", *British Standards Institution*, London.

BSI (1990), "BS5950 Structural use of steelwork in building, Part 3: Design in composite construction, Section 3.1: Code of Practice for Design of Simple and Continuous Composite Beams", *British Standards Institution*, London.

Chaallal, O., Gauthier, D. and Malenfant, P. (1996), "Classification methodology for coupled shear walls", *J. Struct. Eng.*, **122**(12), 1453-1458.

Collins, M.P. and Mitchell, D. (1991), *Prestressed Concrete Structures*, Prentice Hall, Englewood Cliffs, NJ.

Foley, C.M. and Buckhouse, E.R. (1999), "Method to increase capacity and stiffness of reinforced concrete beams", *Practical Periodical on Structural Design and Construction*, **4**(1), 36-42.

Galano, L. and Vignoli, A. (2000,) "Seismic behavior of short coupling beams with different reinforcement layouts", *ACI Struct. J.*, **97**(6), 876-885.

Harries, K.A. (2001) "Ductility and deformability of coupling beams in reinforced concrete coupled wall", *J. Earthq. Spectra*, **17**(3), 457-478.

Harries, K.A., Cook, W.D. and Mitchell, D. (1996), "Seismic retrofit of reinforced coupling beams using steel plates", *ACI SP-160*, June 1, 93-114.

Jones, R., Swamy, R.N. and Ang, T.H. (1982), "Under- and over-reinforced concrete beams with glued steel plates", *Int. J. Cement Compos. Lightweight Concrete*, **4**(1), 19-32.

Kwan, A.K.H. and Zhao, Z.Z. (2002a), "Cyclic behavior of deep reinforced concrete coupling beams", *Proc. of the Institution of Civil Engineers, Structures and Buildings*, **152**(3), 283-293.

Kwan, A.K.H. and Zhao, Z.Z. (2002b), "Testing of coupling beams with equal end rotation maintained and local joint deformation allowed", *Proc. of the Institution of Civil Engineers-structures and Buildings*, **152**(1), 67-78.

L'Hermite, R. and Bresson, J. (1967), "Concrete reinforced with glued plates", RILEM International Symposium, Synthetic Resins in Building Construction, Paris, 175-203.

Lin, W.S. and Kao, C.C. (2003), "Nonlinear finite element 2d analysis for RC beams strengthened by epoxy bonded steel plates", *Chinese J. Mechanics-Series A*, **19**(4), 409-419.

Oehlers, D.J. (1992), "Reinforced concrete beams with plates glued to their soffits", *J. Struct. Eng.,* ASCE, **118**(8), 2023-2038.

Oehlers, D.J. and Bradford, M.A. (1995), "Composite steel and concrete structural members: Fundamental behavior", Pergamon Press, Oxford, England, November.

Oehlers, D.J. and Bradford, M.A. (1999), "Elementary behavior of composite steel and concrete structural members", Butterworth Heinemann, Oxford, England.

Oehlers, D.J. and Moran, J.P. (1989), "Premature failure of externally plated reinforced concrete beams", *J. Struct. Eng.*, **116**(4), 978-995.

Oehlers, D.J., Nguyen, N.T. and Bradford, M.A. (2000a), "Retrofitting by adhesive bonding steel plates to the sides of RC beams, Part 1: Debonding of plates due to flexure", *Struct. Eng. Mech.*, **9**(5), 491-504.

Oehlers, D.J., Nguyen, N.T. and Bradford, M.A. (2000b), "Retrofitting by adhesive bonding steel plates to the sides of RC beams, Part 2: Debonding due to shear and design rules", *Struct. Eng. Mech.*, **9**(5), 505-518.

Pala, S. and Ozmen, G. (1995), "Effective stiffness of coupling beams in structural walls", *Comp. Struct.*, **54**(5), 925-931.

Paulay, T. and Bull, I.N. (1971), "Shear effects on plastic hinges of earthquake resisting reinforced concrete frames", *Struct. Concrete Seismic Actions*, 165-172.

Stafford Smith, B. and Coull, A. (1991), *Tall Building Structures: Analysis and Design*, John Wiley & Sons, Inc.

Su, R.K.L. and Zhu, Y. (2005), "Experimental and numerical analyses of external steel plate strengthened reinforced Concrete Coupling Beams", *Eng. Struct.,* **27**(10), 1537-1550.

Subedi, N.K. (1991), "RC-coupled shear wall structures, I: analysis of coupling beams", *J. Struct. Eng.*, **117**(3), 667-680.

Subedi, N.K. and Baglin, P.S. (1998), "External plate reinforcement for concrete beams", *J. Struct. Eng.*, **124**(12), 1490-1495.

Subedi, N.K., Marsono, A.K. and Aguda, G. (1999), "Analysis of reinforced concrete coupled shear wall

structures", *Struct. Des. Tall Build.*, **8**, 117-143.

Taljsten, B. (1995), "Strengthening of structures using epoxy bounded steel or fibre reinforced plastic plates", IABSE Extending the Lifespan of Structures, August 1995, San Francisco, 1173-1178.

Tassios, T.P., Moretti, M. and Bezas, A. (1996), "On the behavior and ductility of reinforced concrete coupling beams of shear walls", *ACI Struct. J.*, **93**(6), 711-720.

Tegos, I.A. and Penelis, G.G. (1988), "Seismic resistance of short columns and coupling beams reinforced with inclined bars", *ACI Struct. J.*, **85**(1), 82-88.

Uy, B. (2002), "Strength of reinforced concrete columns bonded with external steel plates", *Mag. Concrete Res.,* **54**(1), 61-76.

Wang, W.H., Fu, X.D. and Ni, Y. (1992), "Behavior of ceramite concrete coupling beams in shear wall structures under reversed cyclic loading", (in Chinese) *J. Build. Struct.*, **13**(1), 71-78.